

Repository Istituzionale dei Prodotti della Ricerca del Politecnico di Bari

Flood-prone areas assessment using linear binary classifiers based on flood maps obtained from 1D and 2D hydraulic models

This is a post print of the following article

Original Citation:
Flood-prone areas assessment using linear binary classifiers based on flood maps obtained from 1D and 2D hydraulic models / Manfreda, S., Samela, C., Gioia, A., Consoli, G.G., Iacobellis, V., Giuzio, L., Cantisani, A., Sole, A.. - In: NATURAL HAZARDS. - ISSN 0921-030X. - 79:2(2015), pp. 735-754. [10.1007/s11069-015-1869-5]

Availability:
This version is available at http://hdl.handle.net/11589/55904 since: 2021-03-13

Published version
DOI:10.1007/s11069-015-1869-5

Publisher:

Terms of use:

(Article begins on next page)

17 November 2026

Manuscript
Click here to view linked References

Flood-Prone Areas Assessment Using Linear Binary Classifiers based on Flood Maps obtained from 1D and 2D Hydraulic Models

Salvatore Manfreda[1], Caterina Samela[1], Andrea Gioia[2], Giuseppe Gerardo Consoli[1], Vito Iacobellis[2], Luciana Giuzio[1], Andrea Cantisani[1] and Aurelia Sole[1]

[1] Università degli Studi della Basilicata, Via dell'Ateneo Lucano 10, Potenza, Italy.
email: salvatore.manfreda@unibas.it,

[2] Politecnico di Bari, Via E. Orabona 4, Bari, Italy.

(Last modified 10/04/2015)

ABSTRACT

The identification of flood-prone areas is a critical issue becoming everyday more pressing for our society. A preliminary delineation can be carried out by DEM-based procedures that rely on basin geomorphologic features. In the present paper, we investigated the dominant topographic controls for the flood exposure using techniques of pattern classification through linear binary classifiers based on DEM-derived morphologic features. Our findings may help the definition of new strategies for the delineation of flood-prone areas with DEM-based procedures. With this aim, local features - which are generally used to describe the hydrological characteristics of a basin - and composite morphological indices are taken into account in order to identify the most significant one. Analyses are carried out on two different datasets: one based on flood simulations obtained with a 1-D hydraulic model, and the second one obtained with a 2-D hydraulic model. The analyses highlight the potential of each

morphological descriptor for the identification of the extent of flood-prone areas and, in particular, the ability of one geomorphologic index to represent flood inundated areas at different scales of application.

Keywords: flood hazard, DEM, terrain analysis, geomorphic approaches, ungauged basins.

1 INTRODUCTION

Floods, which are becoming more frequent in urban areas, are one of the natural phenomena more difficult to prevent and to deal with, especially in developing countries (Douglas et al., 2012). The remarkable number of inundations that caused, in the last decades, thousands of deaths and huge economic losses, testifies the vulnerability of many Countries to the flood hazard. On one hand, the exposure of human activities is increasing with the expansion of cities, leading to the reduction of the natural water retention capacity of the soil (e.g., Cannon, 1994; Ceola et al., 2014); on the other hand, there is a motivated suspect that the frequency of great floods is increasing with time (e.g., Milly et al., 2002; Prudhomme, 2002). The current situation is pushing the international community to find new strategies to cope with flood hazards.

The European legislation has introduced new policies for the assessment and management of flood risk for territory protection with the Floods Directive 2007/60/EC. This Directive requires Member States to assess the flood risk, mapping the flood extent over their territories, in order to evaluate assets and humans at risk,

and to take adequate and coordinated measures to reduce this risk for a sustainable hydraulic protection of the territory. The European case is just an example of context where the flood risk is felt as a critical issue that should be faced, in terms of planning, at a large scale. For this reason, the definition of procedures able to provide extended description of the flood-prone areas is a growing need in Europe and several other countries. Therefore, much effort is going into the identification of flood-prone areas through the use of time-consuming hydrological/hydraulic simulations.

The patterns of flood inundations are also critical for the ecology of floodplains (Townsend et al., 1998). In fact, the temporal and spatial dynamics of floods may alter the distribution of vegetation and biodiversity of wetlands (Sharitz and Mitsch; 1993). Therefore, the accurate representation of inundation extents, as well as of surface water bodies, is crucial for the management and conservation of wetland ecosystems (Nei et al., 2009; Bridgham et al., 2013).

In this framework, the research has recently shown that the delineation of flood-prone areas can be carried out using simplified methods that rely on basin geomorphologic features (e.g., Nardi et al., 2006; Manfreda et al., 2011; Degiorgis et al., 2012; Manfreda et al., 2014a; Jalayer et al., 2014; De Risi et al., 2014; Papaioannou et al., 2014). Such innovative procedures may provide a preliminary delineation of the flood-prone areas useful for the planning of numerical analyses, and for insurance companies that have a growing interest toward the identification of the assets and population at risk.

This kind of approach may be extremely beneficial in the definition of new procedures for the identification of flooded areas from remote sensing techniques, where the topographic information may be used as external constraint in the adopted

algorithms, that generally rely only on the local slope or the distance to the channel (e.g., Brivio et al., 2002). For instance, Fluet-Chouinard et al. (2014) used the topographic information to generate inundation probability maps for downscaling course-scale remote sensing data.

In particular, Degiorgis et al. (2012) introduced the use of linear binary classifiers to investigate the relationships between several morphological features and the flooding hazard at the catchment scale. In the present work, we extend the number of morphological features investigated, using single local features as well as composite indices (built with the specific aim to represent a metric of flood hazard) derived from Digital Elevation Models (DEMs).

The performances of the selected morphological features on the Bradano River (Southern Italy) are evaluated at different scales of application, using two reference flood inundation maps: one obtained applying a mono-dimensional approach over the entire basin (basin scale) and one obtained using a two-dimensional approach at the basin outlet (local scale). This last represents an extremely interesting study case that has never been considered for geomorphic applications. In fact, most of the applications made since now have only compared morphological features with mono-dimensional simulations over mountainous areas, but it is well known that the most challenging problem for hydraulic studies is represented by flat areas. Hence, the main motivation for this study is the identification of a metric suitable for both mountainous and flat areas.

In recent studies, the best-performing local features, among those adopted, were the difference in elevation between the considered point and the source of risk (H), and the distance from the nearest stream (D). These features have been also applied in the

present study case with a number of additional morphological indices. Results highlighted remarkable differences in the performances of indices and features applied in different contexts. The study allowed to better address the sensitivity of each index with the change of scale, spatial resolution, etc.

2 STUDY AREA

The Bradano River is one of the major rivers of the Basilicata Region (southern Italy), with a drainage area of about 2,765km². The climate is characterized by a dry-sub humid regime with scarce rains and zero base flow during the summer period (see Fiorentino et al., 2007). More than the 77% of the total surface is covered by agricultural areas, and only the 23% by woodlands and semi-natural areas (this information is provided by the CORINE-Land Cover map of the European Environmental Agency). The upper basin is characterized by a marked topography; by contrast, the terminal portion of the basin, close to the outlet, is extremely flat.

This river basin is one of the most critical in terms of flooding for both the Basilicata and the contiguous Puglia Region. It produced several floods, causing significant damages especially in the portion of the basin close to the river outlet to the Ionian Sea. The first documented flood of the Bradano River refers to the 1827, when two bridges were destroyed interrupting the connection from the South to the City of Matera (this historical event is documented in the archives of the Kingdom of the Two Sicilies under Ferdinando II). Later on, a dramatic event occurred in 1959 when the cities near the coast were significantly damaged and several buildings were destroyed. More recently, flooding also occurred in 1972, 2004 and 2011 (see Figure 1), producing inundations in the outlet portion of the river basin, which is

89 characterised by gentle slopes and flat surfaces. Some additional information on the
90 damages produced by most of these events can be found on http://www.evalmet.it/.
91
92 ## *3 METHODS AND DATASETS*

93 ### 3.1 Flood Maps

94 The extent of the inundated areas was studied by the River Basin Authority of
95 Basilicata (RBAB), that mapped all the rivers of this region. The complex
96 morphological characteristics of the basin forced the RBAB to use both one-
97 dimensional (1D) and two-dimensional (2D) hydraulic models for flood mapping.
98 The first was used for flood propagation along the main river, while the 2D model
99 application was limited to a smaller portion of the river basin nearby the outlet (about
100 80km^2) characterised by extremely flat surfaces, in order to reduce the computational
101 efforts.
102 Two-dimensional models allow studying flood propagation in the areas where it is not
103 possible to recognize a prevailing direction of the water flow. Nevertheless, these
104 models are computationally intensive and for this reason their application is generally
105 limited to a portion of a river basin, while 1D models allow providing a more
106 extensive description of the flood extent at the basin scale. In fact, in the present case
107 the evaluation of the flood-prone areas for a given return period for the main river
108 was carried out by the use of the HEC-RAS model (HEC-RAS, 2010), which is less
109 reliable when dealing with the flat portion of the river basin. Therefore, the basin
110 outlet was investigated by using a 2D approach. Both maps were obtained using a
111 synthetic hydrograph derived from regional analyses assuming a return period of 30
112 years. The flood peak was calculated using the VAPI methodology (Claps et al.,

1999), while the synthetic hydrograph was obtained exploiting the synthetic flow hydrograph proposed by NERC (1975) and modified by Fiorentino & Margiotta (1999).

It is necessary to remark that the RBAB's studies are limited to a portion of the basin that includes the main River, but several tributaries are not analyzed. Therefore, it is highly desirable to have a tool able to provide an extensive characterization of the flood hazard over the entire river network. With this aim, we explored the use of binary classifiers exploiting the two flood maps that refer to the same basin, but differ for reference scale, DEM resolution and methodology adopted for flood mapping.

In order to clarify the procedure used by the RBAB to delineate flood maps, it is useful to provide some additional information about the models adopted. One model is HEC-RAS that probably does not require further descriptions, being a widely used software well documented on the web page of US army Corps of Engineers (http://www.hec.usace.army.mil). On the contrary, it seems appropriate to provide additional information about the 2D hydraulic model named FLORA-2D (FLOod and Roughness Analysis) recently introduced by Cantisani et al. (2012, 2014).

3.2 FLORA-2D

FLORA-2D was developed recently within a collaboration between the University of Basilicata and the company "Research on Energy System" (RSE spa). It has been developed with the aim to simulate flood propagation in flat areas taking into consideration the dynamic effect of vegetation. In fact, flow resistance due to vegetation can be a dominant factor in the inundation process for relatively shallow inundation (<1 m).

137 FLORA-2D has the capability to simulate the inundations considering the spatial and
138 temporal variation of the resistance due to vegetation. Each node of the
139 computational matrix has a roughness coefficient depending on the type of
140 vegetation, flow depth and velocity. In particular, the Manning coefficient n is
141 calculated according to Petryk and Bosmajian (1975) when the vegetation is rigid,
142 and Freeman et al. (2000) in the case of flexible vegetation. The general algorithm
143 governing the flood propagation is based on the "shallow water equations" simplified
144 by neglecting the convective terms.
145 The model has been validated over the Bradano river using flood maps obtained from
146 satellite data. This kind of procedure is becoming more common with the increased
147 potentials of remote sensing products (see e.g., Frappartet al., 2005; Iacobellis et al.,
148 2013, Domeneghetti et al., 2014). An example of a remote sensed image for the flood
149 event of March 2011 is given in Figure 1.A, which has been used by Cantisani et al.
150 (2014). Model reliability has been further investigated using for comparison the
151 model Mike21 HD by the Danish Hydraulic Institute, FLO-2D by O'Brien (2007),
152 FLATModel by Medina et al. (2007). In all cases, the results were comparable in
153 terms of flood extent, but with the great advantage of a significant reduction of the
154 computational costs.
155 In the present application, the computational domain was defined by a square grid
156 with resolution of 10m, while the time step was set to 2sec. This resolution provides a
157 good compromise between simulation time and data accuracy for a correct
158 representation of the process (Sole et al., 2011). It was also observed that the time
159 step of 2s ensures the model stability.
160 The above-mentioned hydrograph was assigned as upstream boundary condition,

while a constant water level equal to 0.5 m a.s.l. was considered as downstream boundary condition (the sea level is assumed slightly above the ordinary conditions). Finally, the spatial distribution of the flow resistance was derived from LiDAR data, used to generate maps of vegetation height (Cobby et al., 2001).

3.3 Digital Elevation Models

Digital Elevation Models (DEMs) contain a significant amount of information that may be helpful for the delineation of flood-prone areas (see e.g., Manfreda et al., 2014).

In the present case, we used, for the entire river basin, the USGS HydroSHEDS (Hydrological data and maps based on SHuttle Elevation Derivatives at multiple Scales-hydrosheds.cr.usgs.gov/index.php) elevation data, available for the entire globe at a fairly good resolution; instead for the portion of the basin outlet we adopted a high resolution LIDAR-derived DEM.

Figure 2 provides a graphical description of the investigated area; in particular, Figure 2.A describes the digital elevation model of the Bradano river basin (called SRTM DEM), extracted from HydroSHEDS (hydrosheds.cr.usgs.gov/index.php) and Figure 2B shows the digital elevation model at the outlet (called LiDAR DEM) of the same basin, extracted from a LiDAR high-resolution DEM and resampled to a 10m x 10m grid.

HydroSHEDS DEMs are derived from remote sensed elevation data of the NASA Shuttle Radar Topography Mission (SRTM). The original SRTM data have been conditioned using a sequence of automated procedures: a DEM–VOID has been released, where the no-data voids have been filled and the main elevation inconsistencies removed. Furthermore, a DEM–CON is also available for

185 hydrological applications; it has been further conditioned in order to accurately
186 reproduce the actual river network. The conditioning process alters the original
187 elevation data and this limits the use of the DEM–CON to drainage network
188 identification procedures. Both the mentioned DEMs have been used for the Bradano
189 River, with a resolution of 3 arc-second that corresponds, for the current study area,
190 to a square grid size of about 90m.
191 The LiDAR high-resolution DEM, instead, was obtained combining airborne LiDAR
192 survey and field measurements that were carried out specifically for the RBAB,
193 paying particular attention to position and elevation of levees. The laser scanning
194 survey was carried out with a density of point equal to 0.7 points/m^2.
195 Figure 3 provides a representation of the standard flood maps used as reference for
196 the application of the linear binary classification. In particular, Figure 3.A shows a
197 flood map derived using a one-dimensional approach over the entire Bradano River,
198 instead Figure 3.B provides a representation of the flooded areas identified by the
199 application of the FLORA-2D model at the outlet of the Bradano basin.

200 **3.4 LINEAR BINARY CLASSIFIERS AND ROC ANALYSIS**

201 Techniques of pattern classification are used to compare DEM-derived quantitative
202 morphologic features and existing flood hazard maps. The linear binary classifiers
203 represent a useful tool for the scope, allowing a quantitative comparison between two
204 binary maps (see Degiorgis et al., 2012). In particular, the flooded areas are easily
205 converted into a binary map assigning a code 1 for flooded areas and a code 0 for
206 marginal hazard areas. The marginal hazard areas are introduced in order to identify
207 the portion of the river basin where a clear distinction between flooded and non-
208 flooded areas is possible. The comparison with morphological features is possible

209 imposing a threshold value to distinguish between the two possible values of the map.
210 In this scheme, the threshold value becomes a parameter that may be changed in
211 order to optimize the performance of each feature.
212 Binary classifiers need to be trained. For this reason, areas predicted as flooded by the
213 use of hydraulic models (one-dimensional over the entire Bradano basin and two-
214 dimensional at the outlet) are used to calibrate the optimal threshold that allows to
215 distinguish flood-prone areas for each selected feature.
216 Single and composite morphologic features are scaled in normalized features lying
217 between -1 and 1. Different normalized thresholds are applied to each normalized
218 features obtaining a binary map of 0 and 1. Comparing this map with the flood map
219 obtained by the hydraulic model, there are four possible conditions in each point of
220 the map: if the threshold detects a flooded area when this condition is present, the
221 point is counted as a true positive; otherwise, if it classifies a point as non-flooded
222 (negative), it is counted as a false negative. If the site is defined non-flooded by the
223 inundation map and it is classified as negative, it is counted as a true negative;
224 otherwise, if it is classified as positive, it is counted as a false positive.
225 The quality of each binary classifier is evaluated using the Receiver Operating
226 Characteristic (ROC) curves that represent a good measure of performance. The ROC
227 graphs are obtained by varying the threshold of the classifier and are defined as the
228 set of pairs of true positive rate (plotted on the Y axis) and false positive rate (plotted
229 on the X axis). ROC curves are also used to select a suitable threshold value (see
230 Fawcett, 2006).
231 We recall that the true positive rate (also called hit rate) is estimated as:
232

$$r_{tp} \approx \frac{Positives\ correctly\ classified}{Total\ positives} \quad [1]$$

The false positive rate (also called false alarm rate) of the classifier is:

$$r_{fp} \approx \frac{Negatives\ incorrectly\ classified}{Total\ negatives} \quad [2]$$

The diagonal line y = x represents the strategy of randomly guessing a class. Any classifier that appears in the higher left triangle performs better than random selection. The best value of the normalized threshold is obtained by minimizing the sum of the false positive rate and the false negative rate r_{fp} + (1 - r_{tp}) assigning equal weights to the two rates.

In order to compare different kinds of binary classifiers, a common method to reduce ROC performance to a single scalar value is to calculate the Area Under the ROC Curve, abbreviated AUC. The value of the AUC ranges from 0.5 (completely random classifier) to 1.0 (perfectly discriminating classifier).

3.4.1 SINGLE FEATURES

In the present section, we provide a synthetic description of the DEM-derived morphologic features adopted in the present study. Among all possible features, we considered the same list adopted by Degiorgis et al. (2012):

1. the upslope contributing area, A_s [m^2];

2. the surface curvature, $\nabla^2 H$ [-], defined as the Laplacian of the elevation;

255 3. the local slope, *S* [-], estimated as the maximum slope among the eight possible
256 flow directions that connect the cell under exam to the adjacent cells;
257 4. the distance from the nearest stream, *D* [m], defined as the length of the path that
258 hydrologically connects the location under exam to the nearest element of the
259 reference drainage network;
260 5. the elevation to the nearest stream, *H* [m], computed as the difference between the
261 elevation of the cell under exam and the elevation of the final point of the above-
262 identified path.
263 A description of these features computed for the Bradano River Basin is given in
264 Figure 4, where one can observe the plots obtained using the DEM at 90m of
265 resolution in Figure 4.A (for the entire basin), while the features obtained for the
266 basin outlet with a DEM at 10m of resolution are given in Figure 4.B. It is necessary
267 to specify that in this last case features like the contributing area have been corrected
268 in order to avoid border effects assigning to the channel cells on the border values
269 derived from the larger DEM.
270

271 **3.4.2 COMPOSITE INDICES**

272 In addition to the mentioned features, a number of composite indices have been also
273 used. Some of these indices are taken from the literature and others have been defined
274 with the aim to describe the relative distance between the water surface during a flood
275 and the local elevation (see Manfreda et al., 2014b). In particular, we adopted the
276 following indices:
277

278 ▪ The modified topographic index, TI_m, first introduced by Kirkby (1975), has
279 proven to be a good indicator for the delineation of areas exposed to flood
280 inundation (Manfreda et al., 2011). This index takes the form:

281 $$TI_m = \ln\left(\frac{A_d^n}{\tan(\beta)}\right), \quad [3]$$

282 where A_d [m]is the drained area per unit contour length, tan(β) is the local gradient,
283 n is an exponent <1.

284

285 ▪ The downslope index, DW_i, proposed by Hjerdt et al. (2004) represents a new way
286 of estimating the hydraulic gradient. The method does not use the exit point at the
287 stream as reference; instead, it calculates how far (L_d [m]) a parcel of water has to
288 travel along its flow path to lose a certain amount of potential energy (d [m]). This
289 index is defined as:

290 $$\tan(\alpha_d) = \frac{d}{L_d}, \quad [4]$$

291 where d was set equal 5m in the present case.

292

293 ▪ H/D: it is obtained by calculating the ratio between the flow distance D and
294 elevation difference H.

295

296 ▪ ln[$h(A_s)/H$]: this index aims to compare in each point a variable water depth h with
297 the elevation difference H, where h is calculated for each basin cell assuming a
298 scaling relationship with the contributing area (A_s) by using an hydraulic scaling
299 relation:

300 $$h(A_s) \approx A_s^n, \quad [5]$$

where h is the water depth [m], $A_s$is the upslope contributing area at the point of interest [m^2], n is the exponent (dimensionless) set equal to 0.3 (see e.g. Nardi et al., 2006).

- ln[$h(A_r)/H$]: this index is similar to the previous one, but in this case h is computed as a function of the contributing area A_r in the section of the drainage network hydrologically connected to the point under exam (see figure 4).

- $[h(A_r) - H]/\ tan(\alpha_d)$: this index aims to describe, in each point of the investigated basin, the change between water depth $h(A_r)$ and the elevation difference H divided by a surrogate of the hydraulic gradient represented by the downslope index.

- $[h(A_r) - H]/D$: this index aims to describe, in each point of the investigated basin, the change between water depth $h(A_r)$ and the elevation difference H divided by the distance D.

All the indices and features are standardized in order to assume a value included in the range -1 and 1.

Figure 6 provides a visual description of the introduced indices computed for the entire Bradano River basin (A) and the Bradano outlet (B). It is necessary to state that the present list of indices was developed by the authors with the specific aim of identifying an hydraulic metric able to account for the main features affecting flood

diffusion on the landscape. These indices have been tested also on the Tiber River in Manfreda et al. (2014b).

4 RESULTS AND DISCUSSION

All suggested features and composite indices have been used to explore their individual ability to describe flood hazard in the Bradano River basin. Given the strong morphological differences existing between the main river and its terminal part, it is extremely interesting to compare the performances of indices applied over the two areas.

Figures 7 and 8 show respectively the ROC curves obtained by separately thresholding each feature on the proposed study area for the two datasets previously introduced. In Figures 7, ROC curves are obtained by comparing the proposed features with the flood map of the Bradano basin obtained by using a 1-D hydraulic model, while in Figure 8 by comparing the proposed features with the flood map of the outlet of Bradano basin evaluated using a 2-D hydraulic model. Generally, the best performing parameters are those that minimize the area above the curve or maximize the area under the curve.

The visual comparison of all ROCs highlights the potential of each feature or index in delineating the flood-prone areas in different contexts. The inter-comparison of the four panels presented in Figure 7 and 8 allow stating that:

i. Among all single features considered the difference in elevation between the considered point and the source of risk (H), and the distance from the nearest stream (D) generally perform better. In fact, the ROC curve of such features has a very large AUC in the first area (Figure 7A).

ii. The behaviour of single features is different in the two considered study cases. In particular, they lower significantly their performances when applied to the flat area of the basin outlet (see Figure 8A).

iii. Among the composite indices, the best performing ones are the ln($h(A_s)/H$) and the ln[$h(A_r)/H$] indices for the main river (application of 1-D hydraulic model over the entire Bradano river) and ln[$h(A_r)/H$] and [$h(A_r) - H$]/D indices for the basin outlet (see Figure 7B and 8B).

iv. The composite index, ln[$h(A_r)/H$], provides similar performances in the two study areas considered herein, and therefore seems the most promising metric among those considered since now.

It is interesting to underline that the single features become less sensitive when dealing with a flat landscape and even features like *H* and *D,* that generally are well suited for flood mapping in several context, here seem to fail. The reason is certainly due to the specific morphological complexity of the area that probably cannot be characterized by this simple metric. On the other hand, the composite index, ln[$h(A_r)/H$], is able to reproduce closely the flood map derived both in the flat area and also over the entire river basin.

In order to provide a quantitative description of the quality of each classifier, we summarize in Tables 1 and 2 the performance of each feature computed for an optimal threshold value, considering the basin scale and the local scale of application, respectively investigated through the one-dimensional and two-dimensional approach. The optimal threshold values were identified by minimizing the sum of the false positive rate and the false negative rate r_{fp} + (1 - r_{tp}). In particular, Tables (1 and 2) provide the following information: the relative values of the optimal normalized

372 threshold τ, the false positive rate r_{fp}, the true positive rate r_{tp}, the sum $r_{fp} + (1\text{-}r_{tp})$
373 and the area under the curve AUC for each of the presented features for the Bradano
374 River basin.
375 Results show that the index $\ln[h(A_r)/H]$ is consistently one of the best performing
376 indices in both cases. Furthermore, it is really remarkable that the thresholds
377 identified for this index are similar in the two cases considered herein, while other
378 features or indices show a larger variability of the performances and of the threshold
379 values calibrated in the two considered cases. This result is particularly significant
380 considering the change of scale of the two DEMs and also the reference hydraulic
381 models adopted. This result may be somehow due to the fact that this index try to
382 resample a physical property of flooding that is independent from the scale and the
383 morphological characteristics of the study area. All this should be explored in
384 additional study cases, but it is extremely stimulating if confirmed, because it would
385 demonstrate the great advantage of this methodology, that could allow to extend the
386 flood mapping over large areas starting from the study of a small portion of the basin
387 and using any kind of hydraulic model for the calibration of the method.
388 An example of application of the procedure over the Bradano River basin is given in
389 Figure 9A and B, where we identified the portion of the basin that have a value of the
390 $\ln[h(A_r)/H]$ index above the calibrated threshold. The maps obtained using the
391 $\ln[h(A_r)/H]$ index provided good performance in both the analysed contexts. After the
392 calibration of the optimal thresholds of this index, the flood hazard has been extended
393 over all tributaries, obtaining a realistic description of the flood prone areas that may
394 be extremely useful for the local River Basin Authority to extend their knowledge
395 about flood hazard.

5 CONCLUSION

The present study investigates the role of different morphological descriptors in the identification of flood-prone areas over the Bradano River basin. In particular, the performances of the proposed features are evaluated using a linear binary classifier and ROC analysis at two different scales of application: at the entire basin scale, using for comparison a flood map derived by a one-dimensional simulation, and in a flat zone of the river basin, exploiting a flood map derived by a two-dimensional model (FLORA-2D). Among the local features, the best performing ones are the difference in elevation between the considered point and the source of risk (H), and the distance from the nearest stream, D; instead, among the composite indices the ones performing better are the $\ln[h(A_s)/H]$ and $\ln[h(A_r)/H]$. In particular, this last seems to be more consistent and less sensitive to the change of resolution in the adopted DEM, the reference hydraulic map used for calibration, and the different topography of the training area. It also provides a reliable representation of the flood-prone areas even in the case of flat areas, where other indices or features become less and less sensitive. The outcomes of the present study are particularly promising, especially considering the number of artificial modifications that characterize the Bradano River.

Acknowledgements: We would like to acknowledge the valuable contribution of the two anonymous reviewers. This research was carried out within the framework of activities of the CINID under the research agreement with the Civil Protection of the Basilicata Region.

REFERENCES

Bridgham SD, Cadillo-Quiroz H, Keller JK, & Zhuang Q (2013) Methane emissions from wetlands: Biogeochemical, microbial, and modeling perspectives from local to global scales. Global Change Biology, 19(5), 1325–1346.

Brivio PA, Colombo R, Maggi M & Tomasoni R (2002) Integration of remote sensing data and GIS for accurate mapping of flooded areas, International Journal of Remote Sensing, 23:3, 429-441, DOI: 10.1080/01431160010014729.

Cannon T (1994) Vulnerability analysis and the explanation of "natural" disasters, in A. Varley (ed.) Disasters, development and the environment, Chichester: John Wiley.

Cantisani A (2012). Monitoraggio e modellazione per la protezione dal rischio idraulico in aree pianeggianti mediante lo sviluppo e l'applicazione di modelli bidimensionali e l'utilizzo di strumenti GIS Open Source (Università della Basilicata).

Cantisani A, Giosa L, Mancusi L, Sole A, (2014) FLORA-2D: A New Model to Simulate the Inundation in Areas Covered by Flexible and Rigid Vegetation. *International Journal of Engineering and Innovative Technology*, vol. 3, Issue 8, p. 179-186, ISSN: 2277-3754.Ceola S, Laio F, Montanari A, (2014) Satellite nighttime lights reveal increasing human exposure to floods worldwide, Geophysical Research Letters, Volume 41, Issue 20, pages 7184–7190, 28 October 2014.

Claps P, Fiorentino M., Rapporto di sintesi sulla valutazione delle piene in Italia – Guida Operativa all'applicazione dei rapporti regionali sulla valutazione delle piene in Italia, 1999, Linea 1 Previsione e Prevenzione degli eventi idrologici estremi. CNR – GNDCI Roma.

444 Cobby DM, Mason DC, Davenport IJ, (2001) Image processing of air born scanning
445 laser altimetry for improved river flood modelling, ISPRS Journal of
446 Photogrammetry and Remote Sensing, 56(2): 121-138.
447 De Risi R., Jalayer F., De Paola F. and Giugni M. (2014) Probabilistic delineation of
448 flood-prone areas based on a digital elevation model and the extent of historical
449 flooding: the case of Ouagadougou. Boletín Geológico y Minero,125 (3): 329-340
450 ISSN: 0366-0176.
451 Degiorgis M, Gnecco G, Gorni S, Roth G, Sanguineti M, Taramasso AC (2012)
452 Classifiers for the detection of flood-prone areas using remote sensed elevation data.
453 *J. Hydrol*., 470-471, 302–315.
454 Domeneghetti A, Tarpanelli A, Brocca L, Barbetta S, Moramarco T, Castellarin A,
455 Brath A (2014). The use of remote sensing-derived water surface data for hydraulic
456 model calibration. Remote Sensing of Environment 149, (2014), 130–141.
457 Douglas I, Alam K, Maghenda M, Mcdonnell Y, Mclean L and Campbell J, (2008)
458 Unjust waters: climate change, flooding and the urban poor in Africa, Environment
459 and Urbanization 20: 187, DOI: 10.1177/0956247808089156.
460 Fawcett T (2006) An introduction to ROC analysis. *Pattern Recognit. Lett*. 27, 861–
461 874.
462 Fiorentino M, Manfreda S, Iacobellis V (2007) Peak Runoff Contributing Area as
463 Hydrological Signature of the Probability Distribution of Floods. *Adv. Water Resour*.,
464 30(10), 2123-2134.
465 Fiorentino M, Margiotta MR (1999) La valutazione dei volumi di piena ed il calcolo
466 semplificato dell'effetto di laminazione di grandi invasi, Atti del 19° corso di

467 aggiornamento su "Tecniche per la difesa dall'inquinamento, G. Frega (a cura di),
468 Editoriale Bios, Cosenza, 203-222.
469 Fluet-Chouinard E, Lehner B, Rebelo L-M, Papa F, and Hamilton SK, (2014)
470 Development of a global inundation map at high spatial resolution from topographic
471 downscaling of coarse-scale remote sensing data, Remote Sensing of Environment,
472 http://dx.doi.org/10.1016/j.rse.2014.10.015
473 Frappart F, Seyler F, Martinez J-M, León J G, Cazenave A, (2005) Floodplain water
474 storage in the Negro River basin estimated from microwave remote sensing of
475 inundation area and water levels, Remote Sensing of Environment, 99(4), 387--399
476 http://dx.doi.org/10.1016/j.rse.2005.08.016.
477 Freeman GE, Rahmeyer W, Copeland R R (2000) Determination of Resistance Due to
478 Shrubs and Woody Vegetation, Coastal and Hydraulics Laboratory, ERDC/CHL TR-
479 00-25, U.S. Army Engineer.
480 HEC-RAS 4.1: online available at: http://www.hec.usace.army.mil/software/hec-
481 ras/documentation/HEC-RAS_4.1_Reference_Manual.pdf.
482 Hjerdt KN, McDonnell JJ, Seibert J, Rodhe A (2004). A new topographic index to
483 quantify downslope controls on local drainage. Water Resour. Res., 40, W05602.
484 Iacobellis V, Gioia A, Milella P, Satalino G, Balenzano A and Mattia F (2013) Inter-
485 comparison of hydrological model simulations with time series of SAR-derived soil
486 moisture maps. European Journal of Remote Sensing- 46: 739-757; doi:
487 10.5721/EuJRS20134644.
488 Jalayer F, De Risi R, De Paola F, et al. (2014) Probabilistic GIS-based method for
489 delineation of urban flooding risk hotspots, *Natural Hazards*, ISSN: 0921030X, DOI:
490 10.1007/s11069-014-1119-2.

491 Kirkby MJ (1975) *Hydrograph modelling strategies*, Progress Phys. Hum. Geogr.,
492 69–90.
493 Manfreda S, Di Leo M, Sole A (2011) Detection of Flood Prone Areas using Digital
494 Elevation Models. *J. Hydrol. Eng*., 16(10), 781-790.
495 Manfreda S, Nardi F, Samela C, Grimaldi S, Taramasso AC, Roth G and Sole A,
496 (2014a) Investigation on the Use of Geomorphic Approaches for the Delineation of
497 Flood Prone Areas, *J. Hydrol*., 517, 863-876.
498 Manfreda S, Samela C, Sole A, and Fiorentino M (2014b) Flood-Prone Areas
499 Assessment Using Linear Binary Classifiers based on Morphological Indices.
500 Vulnerability, Uncertainty, and Risk: pp. 2002-2011. doi:
501 10.1061/9780784413609.201.
502 Medina V, Hurlimannn M, Bateman A, Application of FLATModel, a 2D finite
503 volume code, to debris flows in the northeastern part of Iberian Peninsula,
504 Landslides, Springer Verlag Editor, 2007.
505 Milly PCD, Wetherald RT, Dunne KA, Delworth TL (2002) Increasing risk of great
506 floods in a changing climate. Nature, 415, 514-517.
507 Nardi F, Vivoni ER, Grimaldi S (2006) Investigating a floodplain scaling relation
508 using a hydrogeomorphic delineation method. Water Resour. Res., 42, W09409.
509 Nel JL, Roux DJ, Abell R, Ashton PJ, Cowling RM, Higgins JV, Thieme M, Viers JH
510 (2009) Progress and challenges in freshwater conservation planning. Aquatic
511 Conservation: Marine and Fresh water Ecosystems, 19(4), 474–485.
512 O'Brien J, FLO-2D User Manual. Version2007.06.

513 Papaioannou G, Vasiliades L, Loukas A (2014) Multi-Criteria Analysis Framework
514 for Potential Flood Prone Areas Mapping, J Water Resources Management, Springer
515 Netherlands, http://dx.doi.org/10.1007/s11269-014-0817-6.
516 Petryk S, Bosmajian G B (1975) Analysis of flow through vegetation, Journal of the
517 Hydraulics Division, ASCE, 101(7): 871-884.
518 Prudhomme C, Reynard N and Crooks S (2002) Downscaling of global climate
519 models for flood frequency analysis: where are we now?, Hydrol. Process. 16, 1137–
520 1150.
521 Sharitz RR, Mitsch WJ (1993) Southern hardwood forests. In: Martin, W.H., Boyce,
522 S.G., Echtemacht, A.C. (Eds.), Biodiversity of the Southeastern United States:
523 Lowland Terrestrial Communities. Wiley, New York, pp. 311-372.
524 Sole A, Giosa L, Cantisani A, Statuto D, Nolè L (2011) Analisi di sensibilità nella
525 modellazione delle inondazioni di aree pianeggianti - Sensitivity analysis in flood
526 modeling of flat areas, Italian Journal of Engeneering Geology and Environment,
527 Special Issue, pp. 157-167, DOI: 10.4408/IERGE. 2011-01.S-12.
528 Townsend PA, Walsh SJ, (1998) Modeling floodplain inundation using an integrated
529 GIS with radar and optical remote sensing, *Geomorphology*, Volume 21, Issues 3–4,
530 January 1998, Pages 295-312, ISSN 0169-555X, http://dx.doi.org/10.1016/S0169-
531 555X(97)00069-X.
532
533

EntireBradanoBasin - 1D Hydraulic Model					
Single features	**τ**	**r_{fp}**	**r_{tp}**	**$r_{fp}+(1-r_{tp})$**	**AUC**
A_s	-0.999	0.021	0.186	0.834	0.584
D	**-0.928**	**0.178**	**0.784**	**0.395**	**0.882**
ΔH	0.051	0.627	0.897	0.730	0.578
H	**-0.960**	**0.113**	**0.963**	**0.150**	**0.964**
S	-0.956	0.286	0.898	0.388	0.870

Indices	**τ**	**r_{fp}**	**r_{tp}**	**$r_{fp}+(1-r_{tp})$**	**AUC**
Tim	-0.235	0.286	0.899	0.387	0.869
DW_i	-0.980	0.142	0.883	0.259	0.919
H/D	-0.974	0.272	0.812	0.460	0.841
$\ln[h(A_r)/H]$	**-0.422**	**0.143**	**0.939**	**0.204**	**0.950**
$\ln[h(A_s)/H]$	**-0.612**	**0.134**	**0.953**	**0.182**	**0.953**
$[h(A_r)-H]/DW_i$	-0.991	0.790	0.992	0.799	0.654
$[h(A_r)-H]/D$	0.818	0.133	0.874	0.259	0.933

Table 1. Results of the linear binary classifiers for the Bradano River basin: the optimal normalized threshold, τ, the false positive rate, r_{fp}, the true positive rate, r_{tp}, the sum $r_{fp} + (1 - r_{tp})$, and the area under the curve (AUC) for each descriptor. The best performing features are highlighted using bold characters.

Bradano Outlet - 2D Hydraulic Model					
Single features	**τ**	**r_{fp}**	**r_{tp}**	**$r_{fp}+(1-r_{tp})$**	**AUC**
As	-0.991	0.000	0.015	0.985	0.507
D	**-0.842**	**0.247**	**0.458**	**0.789**	**0.625**
ΔH	0.330	0.421	0.458	0.963	0.527
H	**-0.574**	**0.768**	**0.990**	**0.778**	**0.609**
S	-0.986	0.644	0.719	0.926	0.548

Indices	**τ**	**r_{fp}**	**r_{tp}**	**$r_{fp}+(1-r_{tp})$**	**AUC**
TIm	-0.139	0.453	0.531	0.922	0.555
DW_i	0.000	0.142	0.441	0.701	0.609
H/D	-0.755	0.911	0.992	0.919	0.505
$\ln[h(A_r)/H]$	**-0.423**	**0.267**	**0.811**	**0.456**	**0.791**
$\ln[h(A_s)/H]$	-0.809	0.759	0.956	0.803	0.623
$[h(A_r)-H]/DW_i$	-0.068	0.558	0.886	0.672	0.659
$[h(A_r)-H]/D$	**0.471**	**0.221**	**0.734**	**0.487**	**0.798**

Table 2. Results of the linear binary classifier for the outlet of Bradano River basin: the optimal normalized threshold value τ, the false positive rate r_{fp}, the true positive rate r_{tp}, the sum of $r_{fp}+(1-r_{tp})$ and the area under the curve (AUC) for each descriptor. The best performing features are highlighted using bold characters.

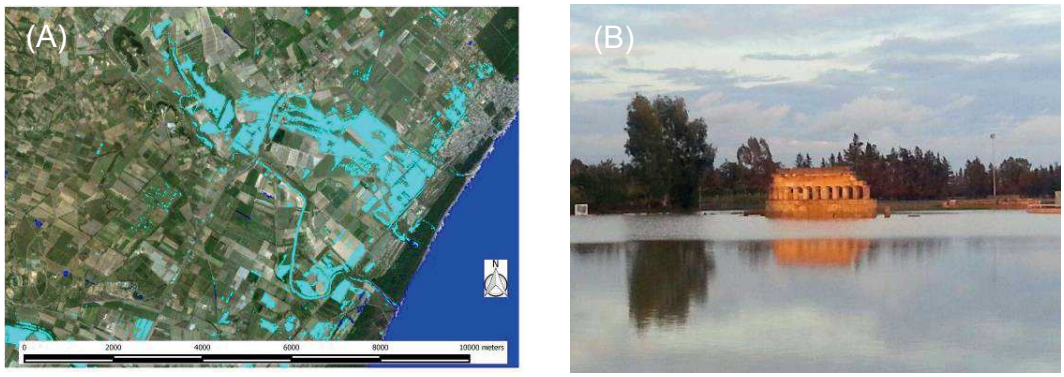


Figure 10. A) Inundated areas during the flood event of March 2011 obtained by processing remote sensed images. B) The Ancient Temple of "Tavole Palatine" flooded by the event of March 2011.

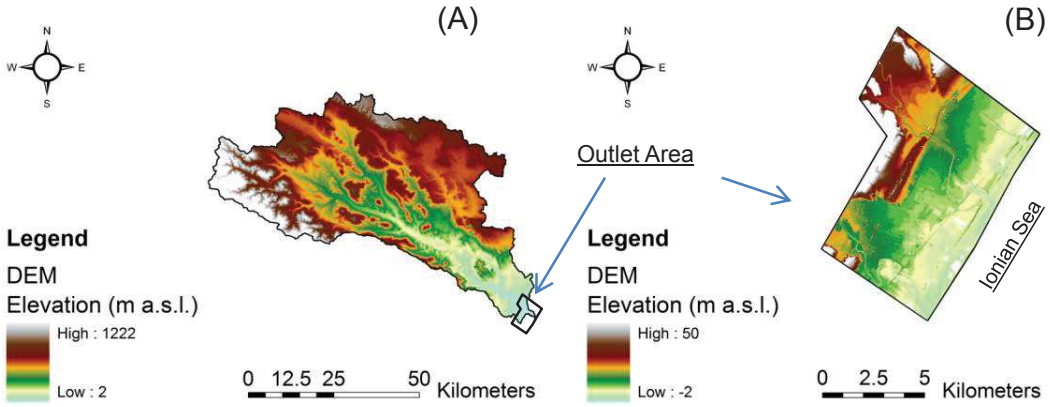


Figure 1. SRTM DEM of the entire Bradano River basin (A). LiDAR DEM of the basin outlet of Bradano River (B).

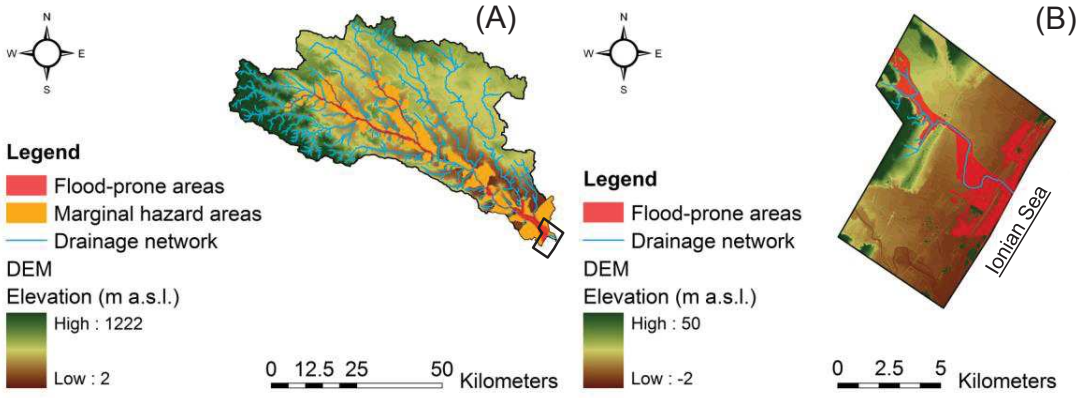
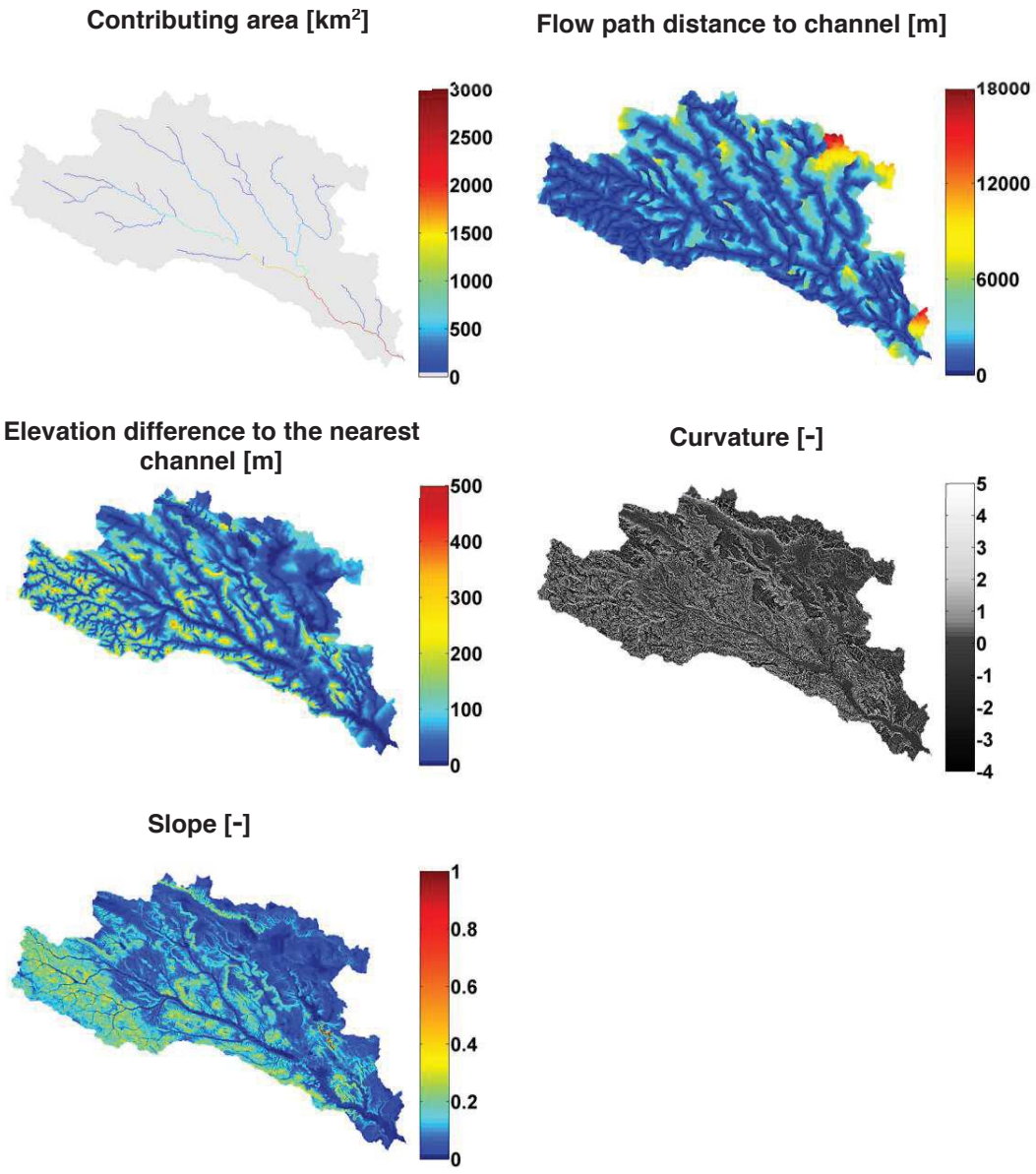
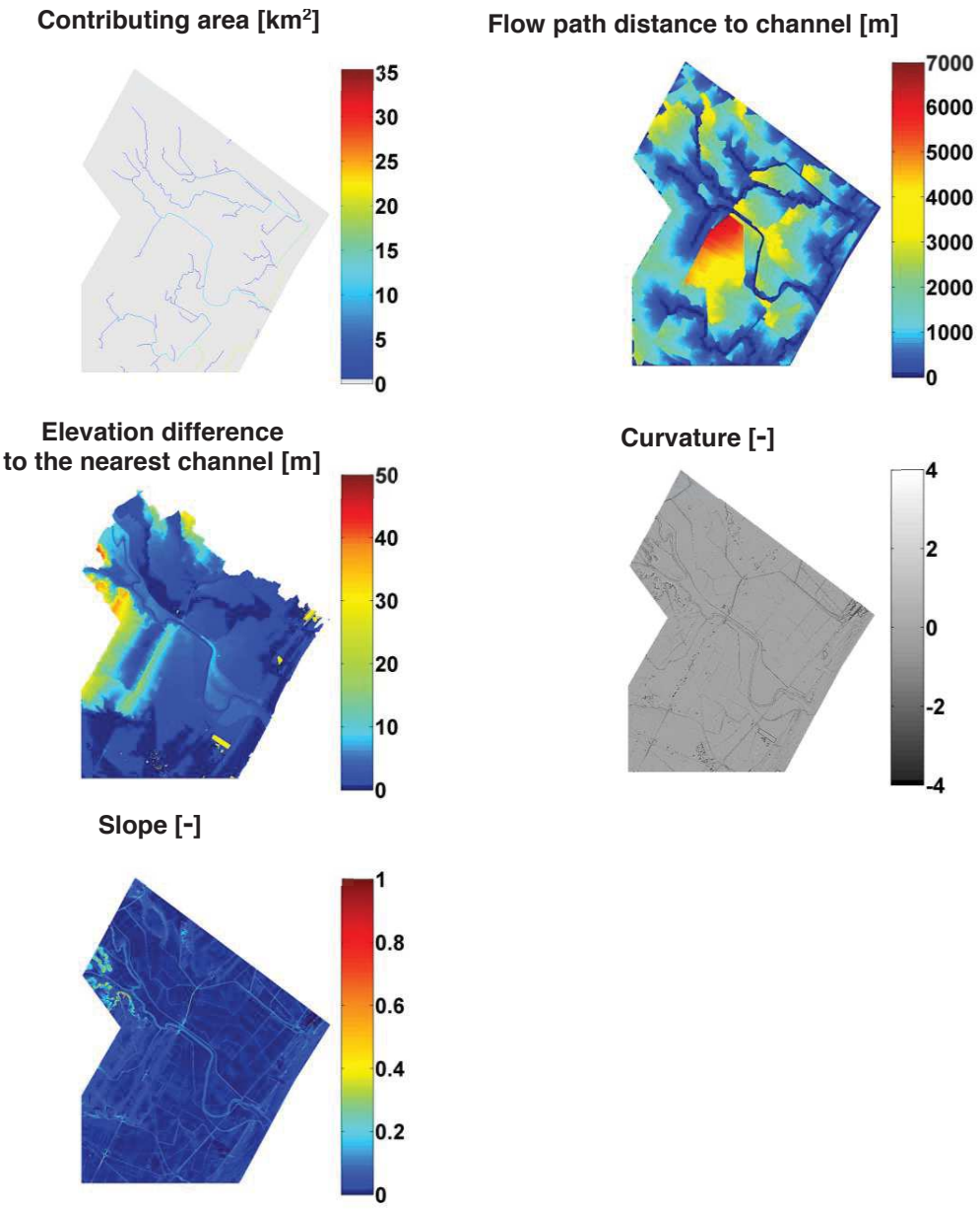


Figure 2. Flood map derived by using a one-dimensional approach over the entire basin of Bradano (A). Flood map derived by using a two-dimensional approach at the outlet of Bradano River basin (B).



560

561 **Figure 3A. Local morphological features estimated for the entire Bradano river basin using the**
562 **SRTM DEM with 90 m of resolution.**



563

564 **Figure 3B. Local morphological features calculated at the outlet of the Bradano basin estimated**
565 **using the LiDAR DEM with 10 m of resolution.**

566

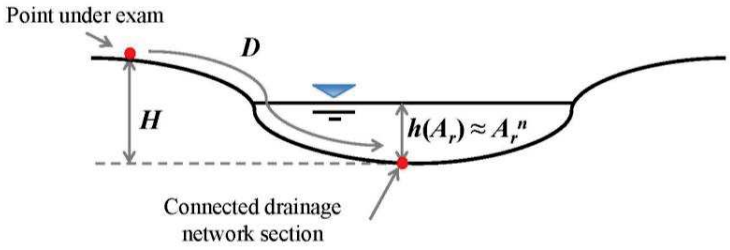
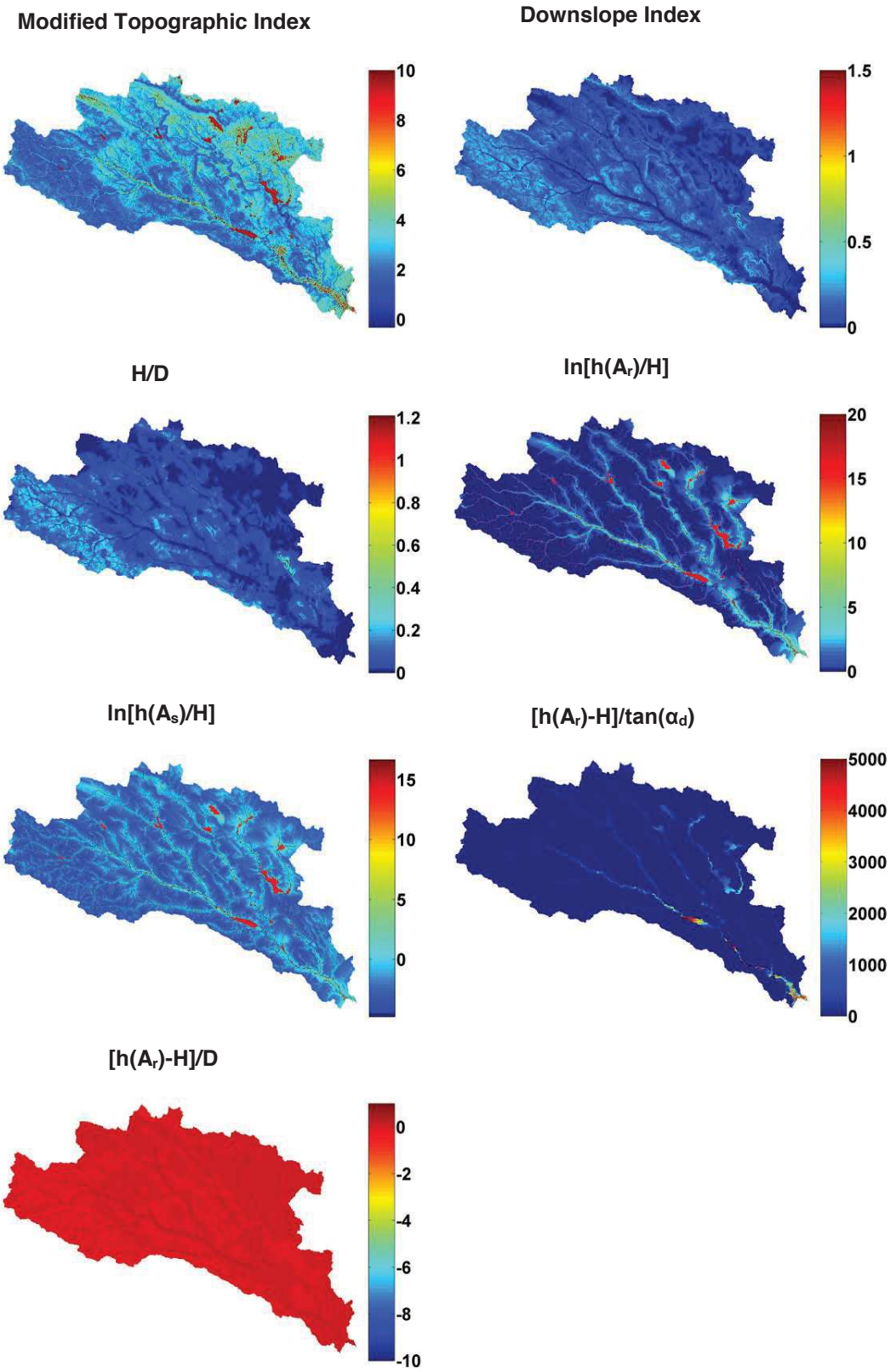


Figure 4. Example of a hydraulic cross-section with the description of the parameters *H* and *h*.



572

573 **Figure 5A. Composite morphological indices estimated for the entire Bradano river basin using**
574 **the SRTM DEM with 90 m of resolution.**

575

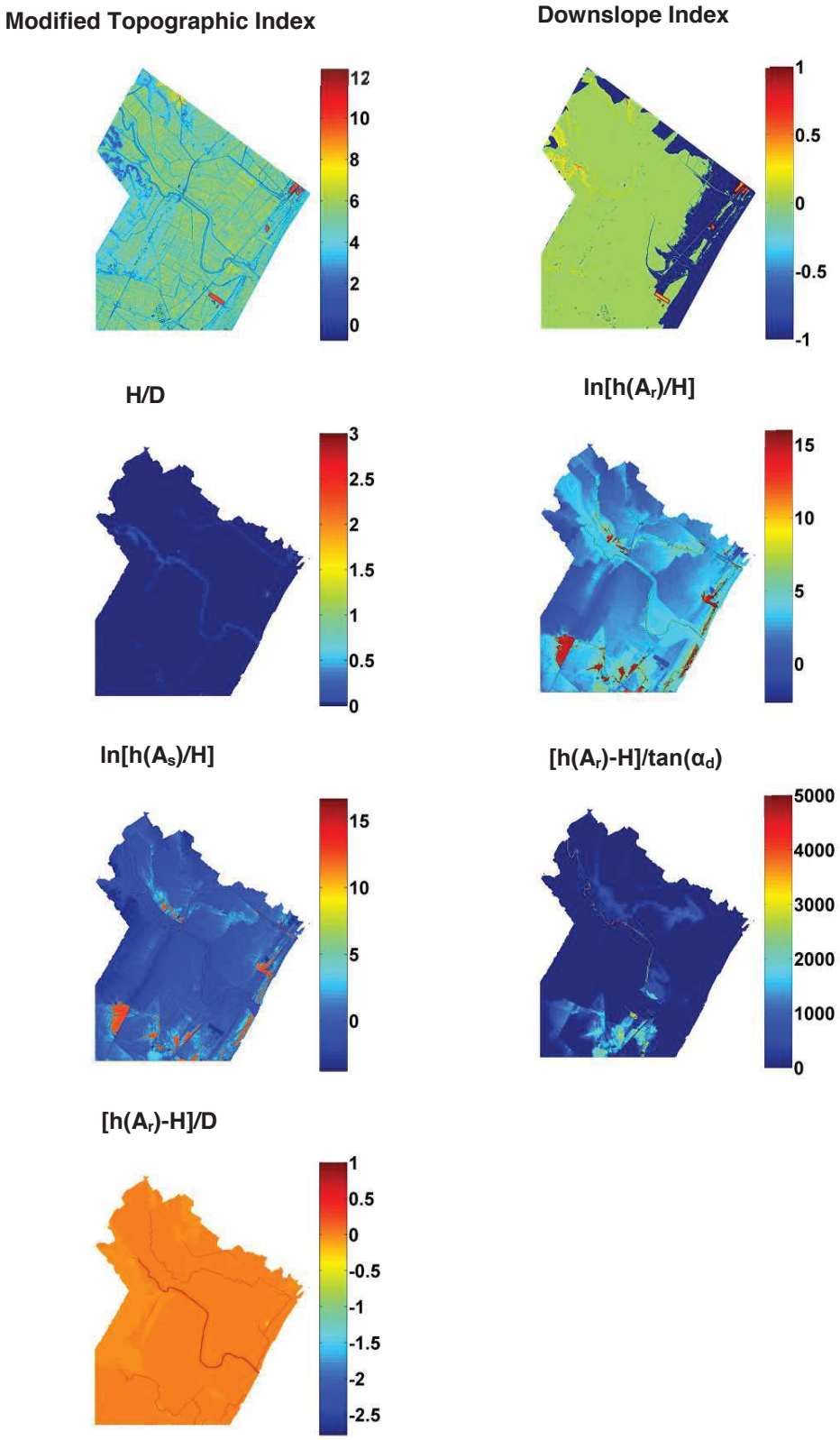
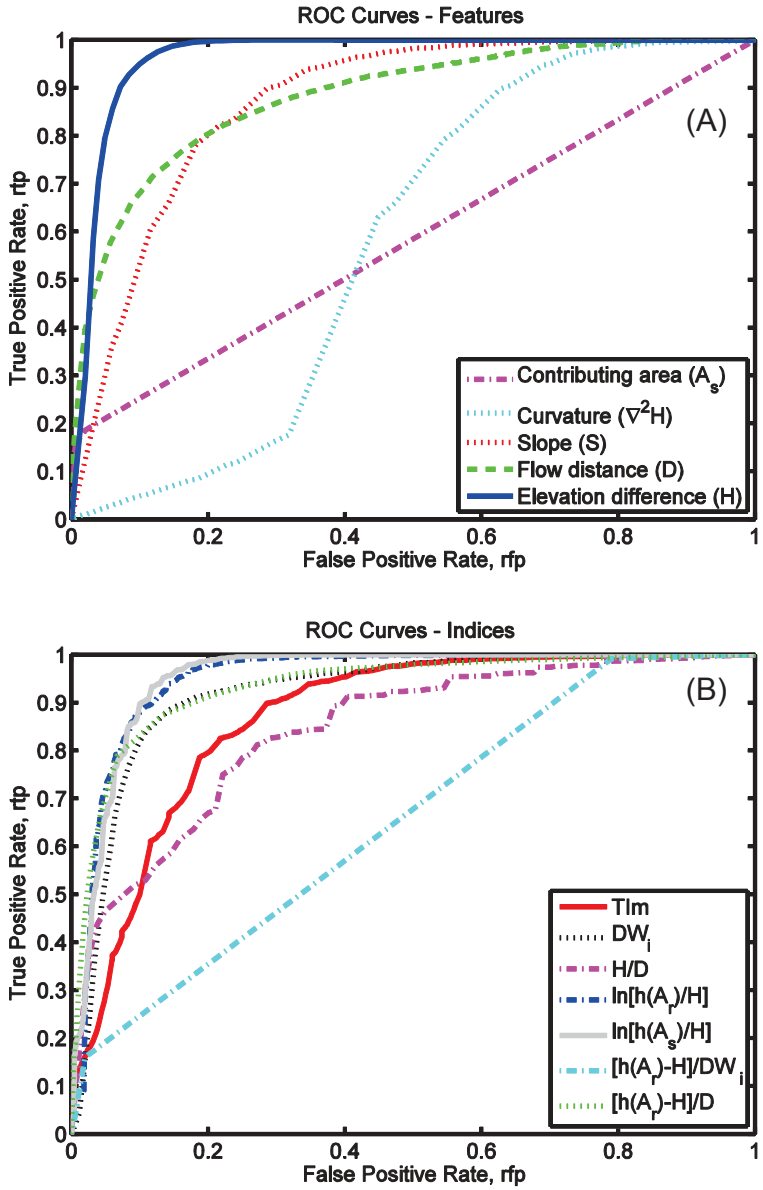


Figure 5B. Composite morphological indices computed at the outlet of the Bradano river basin estimated using the LIDAR DEM with 10 m of resolution.



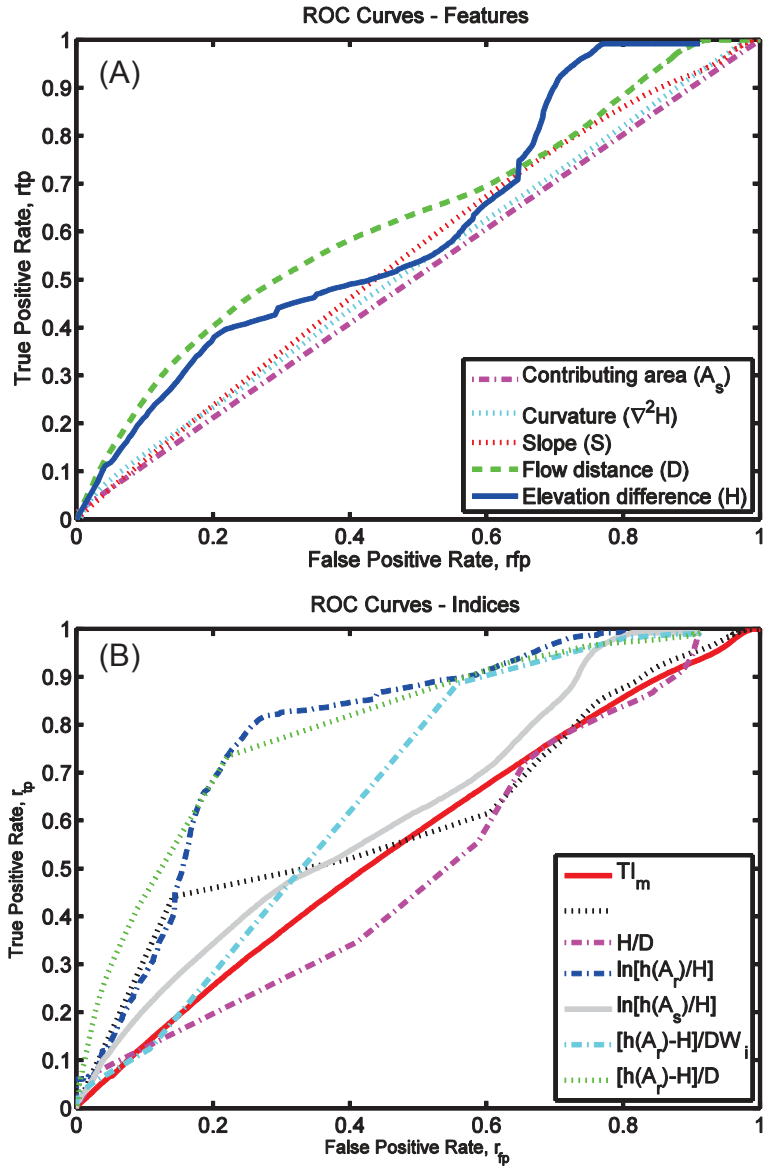
579

580

581

582 **Figure 6. ROC curves obtained for local features (A) and composite indices (B) obtained by**
583 **comparing the proposed features with the flood map of the Bradano basin obtained using the 1-**
584 **D hydraulic model.**

585



586
587
588

589 **Figure 7. ROC curves obtained for local features (A) and composite indices (B) obtained by**
590 **comparing the proposed features with the flood map of the outlet of Bradano basin evaluated**
591 **using the 2-D hydraulic model.**

592

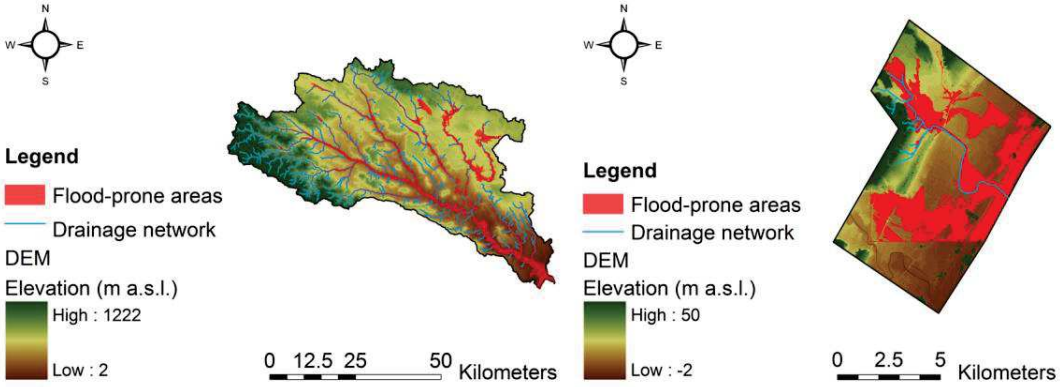


Figure 8. Flood maps of the Bradano River basin obtained using the linear binary classifier based on the index $ln(h(A_l)/H)$ applied on the entire basin (A) and the basin outlet (B).

Additional Material for Editor and Reviewers

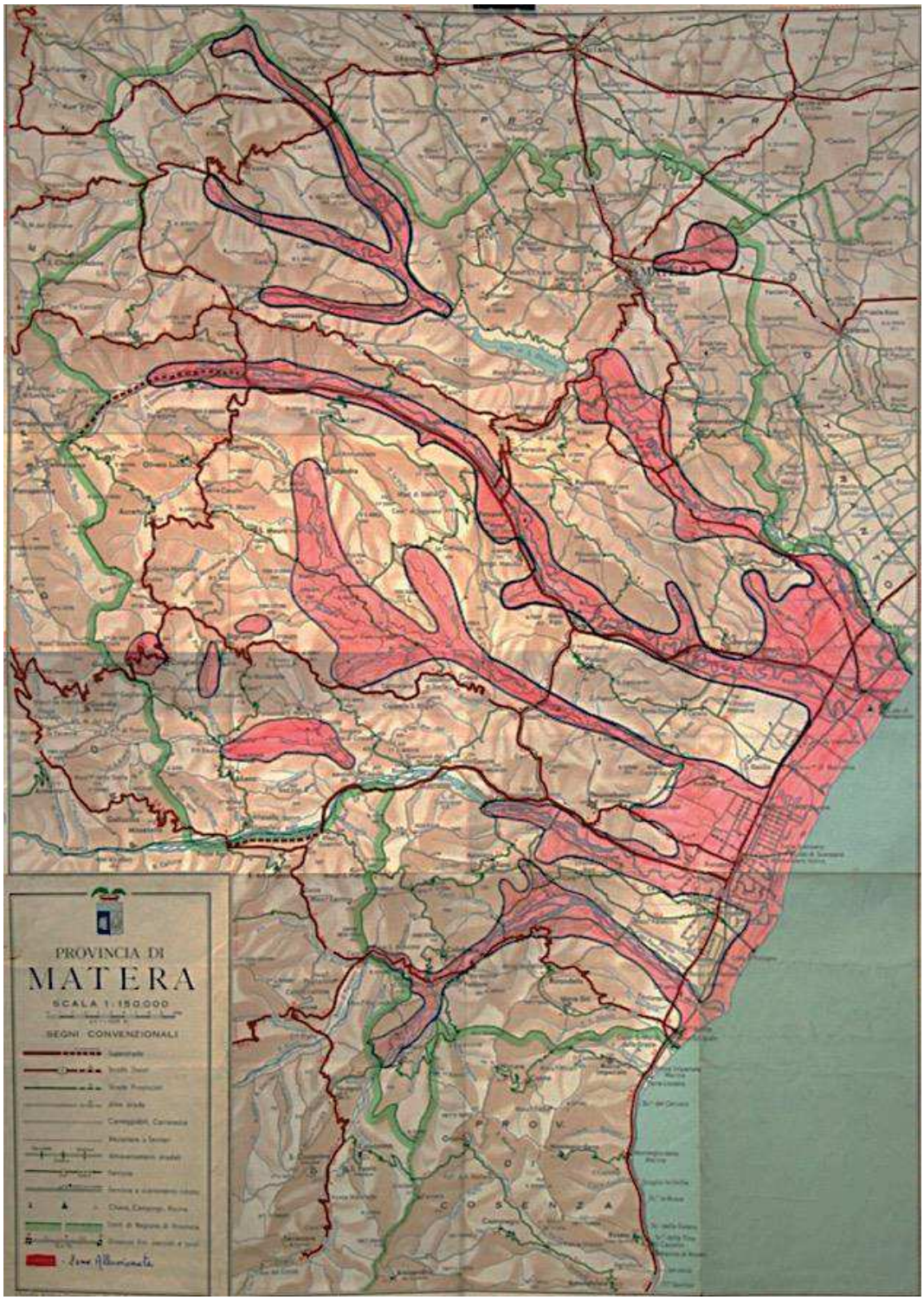


Figure 9. Inundated areas during the flood event of January 1972 edited by the Province of Matera.